Accepted for publication in Composite Structures, doi: 10.1016/j.compstruct.2015.08.016

Effects of hygrothermal stress on the failure of CFRP composites

M. Meng, M. D. J. Rizvi, S. Grove, H. R. Le*

School of Marine Science and Engineering, Plymouth University, United Kingdom

*Fax: +44 (0)1752 586101; email address: huirong.le@plymouth.ac.uk

Abstract

This paper investigates the hygrothermal effects on the failure mechanisms in bending of carbon fibre reinforced polymer (CFRP) composites. Accelerated diffusion testing was carried out by immersion at 50°C constant temperature and 70 bar hydrostatic pressure to study the effects of fresh or sea water diffusion into pre-preg CFRP laminates. Consequently the composite laminates were tested in bending after 1 and 3 months' immersion. A three-dimensional finite element analysis (FEA) model was developed to couple the moisture diffusion, hygrothermal expansion and bending. Optical and field emission scanning electronic microscope (SEM) were employed to analyse the failure mechanisms of CFRP composites in bending after immersion. The study showed that the mechanical properties are significantly reduced after short term immersion due to the edge effects, while the damage to the fibre/polymer interface becomes more significant to laminate degradation after longer-term immersion.

Keywords: CFRP; moisture diffusion; FEA; failure mechanism; interlaminar shear

1. Introduction

Due to their high stiffness and strength to weight ratios, carbon fibre reinforced polymer (CFRP) composites have been widely recognized as potential candidates for many key structures in offshore applications, including renewable energy (wind and current turbines) and naval structures (hulls, masts and propeller shafts)[1, 2]. In such industries, the mechanical structure is designed to have a service life of several decades. Therefore environmental issues should be taken into account in the evaluation of their suitability.

In the marine environment, composites are subjected to moisture and hydrostatic pressure. These environmental conditions have important effects on the polymer matrix in particular, while the fibres are typically not affected as much by moisture or pressure; swelling or contraction of the polymer matrix is resisted by the fibre so that residual (hygrothermal) stress develops in composites [3]. The increase of moisture content may not only cause a gradual reduction of the glass transition temperature, which is often a critical selection factor [4], but also change the stress distribution in the composite laminate. Since the moisture diffusion is time dependant, the hygrothermal stress should be investigated in the time domain. However, few publications of these topics have been found in the literature.

Moisture diffusion in isotropic material, such as pure polymer, is governed by Fick's first and second laws [5]. However, many previous publications, e.g. [6-9], have shown that moisture diffusion in polymer-based composites also follow Fick's laws. According to these previous studies, temperature does not change the saturated moisture content but accelerates the process of diffusion. Shen and Springer [6] pointed out that, for many polymer composites, the temperature distribution approaches equilibrium about one millions times faster than the moisture concentration. Therefore, the short time scale fluctuations in temperature can be neglected compared to the effects of the variation of moisture content.

Previous experimental observations [6, 10] have demonstrated that, for polymer composites, the expansion induced by moisture absorption is generally a linear function of moisture content if the moisture content is less than 2%. This relation is normally used to determinate the coefficient of hygrothermal expansion (CHE) in a unidirectional lamina, and classical laminate theory (CLT) can be employed to calculate the CHE at the laminate level [3]. Since the moisture distribution inside composites is non-uniform throughout any given ply, CLT is unlikely to predict the hygrothermal expansion and the associated stresses for a laminate with a complicated lay-up. The effects of hygrothermal stress on the mechanical properties of laminated composites appear not to have been investigated sufficiently.

The aim of the present work is to investigate the impact of hygrothermal stress on the failure mechanisms of composite materials in bending, by means of experimental and numerical approaches. Fresh water (tap water) and sea water were used for the diffusion test to investigate the effect of NaCl on the degradation of composite properties. A hydrostatic apparatus was used to provide constant 70 bar pressure (equivalent to a water depth of 700 m). In order to accelerate the diffusion process, all the three chambers were placed in an oven at a constant temperature of 50°C. After soaking the samples for one and three months respectively, both the interlaminar shear strength and flexural strength were measured and

compared with that of un-soaked samples. A 3D FEA model was developed to simulate the moisture diffusion, hygrothermal expansion and the coupling of hygrothermal stress and bending. This paper uses the 'forensic' approach: the bending test was carried out until fracture and the measured critical load was input into the FEA model, then the FEA results of stress distribution were used to explain the failure mechanisms observed in the experiment. The combination of FEA modelling and experiment showed the change of hygrothermal stress after various immersion periods and the variation in composite failure modes.

2. Experimental methods

2.1. Material preparation

High strength carbon fibre/epoxy pre-preg (Cytec 977-2-12kHTS) was used in this study. This is a high temperature (180°C) curing toughened epoxy resin with 212°C glass transition temperature (T_g) which is formulated for autoclave moulding. The aromatic epoxide-amine network[11] is constituted of bisphenol A diglycidyl ether (DGEBA) and diaminodiphenyl sulfone (DDS) which is schemed as Fig.1. It can be seen from Fig.1 that the DGEBA contains the hydroxyl radicals which are hydrophilic.

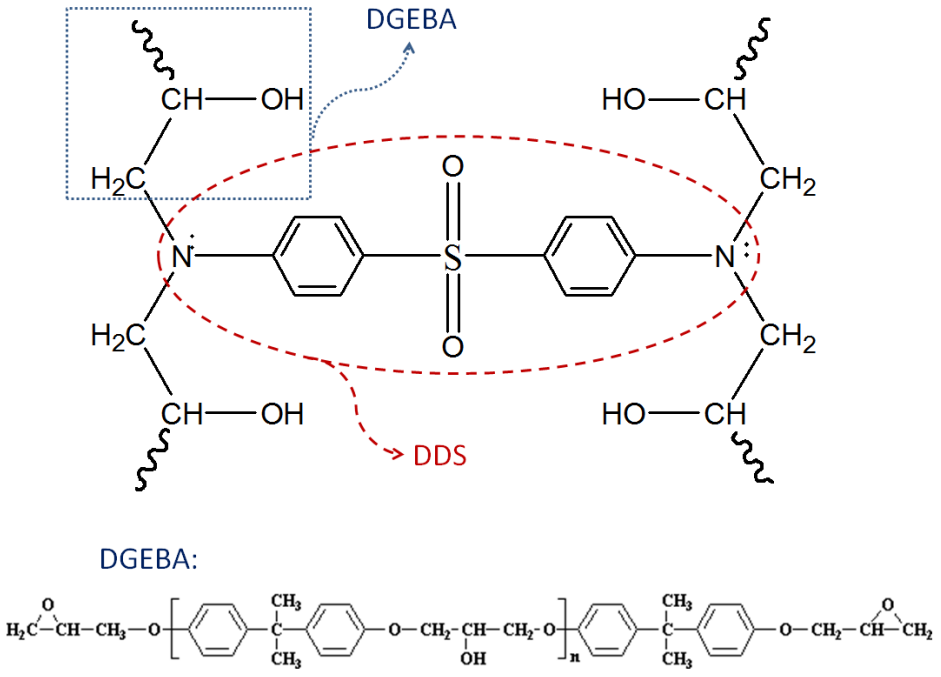

Fig.1. Schematics of crosslink network of 977-2 epoxy resin. The value n is in the range of 0-25.

The pre-preg was laid up on a plane moulding tool and both the pre-preg plates and moulding tool were sealed in a vacuum bag before being put into the autoclave chamber which was under 85psi (0.6MPa) pressure. Following the curing instruction in product technical data sheet [12], a heating ramp rate of 3 °C/min was chosen, followed by 2 hours dwelling at 180°C. The calculated fibre volume fraction was $V_f = 57.9\%$ as described in [15].

Four typical lay-up sequences were chosen for the composite laminates (Table 1). These four lay-ups are the simplest examples of laminates which show a range of different laminate stacking: the unidirectional (UD) and unidirectional transverse (UT) laminates are fibre and matrix dominated which show the strongest and weakest mechanical properties, while the cross-ply (CP) and angle-ply (AP) laminates present intermediate properties. The study of these four common lay-ups could provide a general view of the interplay of fibre orientation and moisture diffusion. The composite laminates were to be tested in bending following the ISO standards [13, 14] which required a nominal thickness of 2 mm. Therefore all of the laminates in present work were made up of 16 plies to satisfy the ISO standards. The two unidirectional (UD and UT) laminates were cut from the same composite plates with different cutting orientations. The cutting pattern is shown in Fig.2. The final thickness of the manufactured plates was not identical. Possible reasons include manufacturing defects and measurement errors which have been discussed in the previous paper [15].

Table 1 Laminate configuration

Laminate	Lay-up	Thickness (mm)	Ply-thickness (mm)
UD	$[0]_{16}$	2.08	0.13
UT	$[90]_{16}$	2.08	0.13
CP	$[90/0]_{4s}$	1.92	0.12
AP	$[\pm 45]_{4s}$	1.92	0.12

UD: Unidirectional (longitudinal); UT: Unidirectional (Transverse); CP: Cross-Ply; AP: Angle-Ply

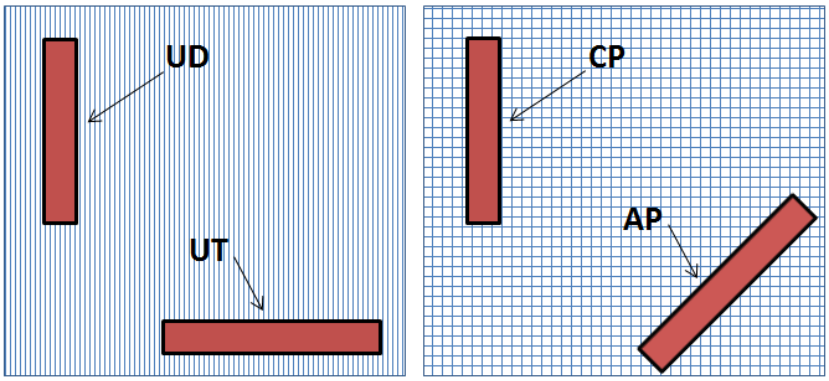

Fig.2. The cutting pattern of the composite laminates. UD and UT laminates were cut from one panel with perpendicular orientation, while CP and AP were from the other.

2.2. Accelerated water diffusion tests

In order to accelerate the water absorption, the chambers were placed in an oven at a constant temperature 50°C. Three chambers were used in the test, containing fresh water (tap water), sea water and sea water at 70 bar hydrostatic pressure respectively. Fig.3 shows the hydrostatic chamber which was used in the diffusion test. The hydrostatic chamber was made of stainless steel providing approximate 20 litres of cylindrical space, and the pressure was applied through the hose by a hydraulic pump. The specimens were constrained and separated

by breathing nylon cloth before being immersed. The sea water was collected from the Atlantic Ocean near Plymouth harbour, and the water was refreshed every month during the tests. The salinity of the sea water was various by seasons and depth, and the values were in range of 3.4%-3.5% in weight. The salinity was similar with the open literatures so that the chemical composition can be referred to the ASTM D1141 [16].

The composite laminates were immersed into the three chambers for the diffusion test. Following the ASTM D5229 [17], the specimens were taken out at intervals to measure the moisture content and hygrothermal expansion. Before being immersed into the water, all of the specimens were oven-dried at 70°C for 48 hours. The moisture content was measured by a weight scale with 0.01 mg accuracy, while the dimension was measured by a vernier calliper with 0.01 mm nominal accuracy.

Fig.3. The hydrostatic chamber used in the diffusion test.

Table 2 Accelerated diffusion test results (50°C**)**

	[a]Immersion	M_{max} (%)	Height (mm)	Length (mm)	Width (mm)	D^{app} (10^{-13} m^2/s)	D_T (10^{-13} m^2/s)	D_L (10^{-13} m^2/s)
$UD[0]_{16}$	Sea	0.81	2.06	204	15	2.6	–	–
	SP	0.89	2.06	204	15	2.6	2.0	3.6
	Tap	0.82	2.06	204	15	2.8	2.2	3.6
[b]$UT[90]_{16}$	SP	0.88	2.06	15	122	2.8	–	–
	Tap	0.82	2.06	15	122	3.0	–	–
$CP[90/0]_{4s}$	Sea	0.89	1.95	286	15	2.8	–	–
	SP	0.92	1.95	286	15	3.0	–	–
	Tap	0.89	1.95	286	15	3.0	–	–
$AP[\pm45]_{4s}$	Sea	0.89	1.95	100	20	2.8	–	–
	SP	0.93	1.95	100	20	2.9	–	–
	Tap	0.89	1.95	100	20	2.9	–	–

(a) ‘Sea’: sea water immersion; ‘Tap’: tap water immersion; ‘SP’: sea water immersion with 70 bar hydrostatic pressure.

(b)The UT laminate was immersed only in Tap and SP conditions.

At least five specimens of each lay-up were immersed in each chamber, and the mean values were calculated. The results are shown in Table 2. The equations used to calculate the apparent moisture diffusivity (D^{app}), longitudinal (D_L) and transverse (D_T) moisture diffusivities are shown in the Appendix. Only UD and UT data were used to extract D_T and D_L for simplicity.

Because the longitudinal elastic modulus of carbon fibre is much higher than epoxy, the longitudinal hygrothermal expansion of the UD laminate is expected to be very small. Indeed, the measured values of the CP and AP laminates were also smaller than the accuracy of vernier calliper, and hence only the specimen with a very long width w (UT laminate) could provide measureable expansion. The increase of hygrothermal expansion as a function of moisture content is shown in Fig. 4. It can be seen from the figure that the hygrothermal expansion of the 'SP specimen' showed a smaller value compared with 'Tap specimen'.

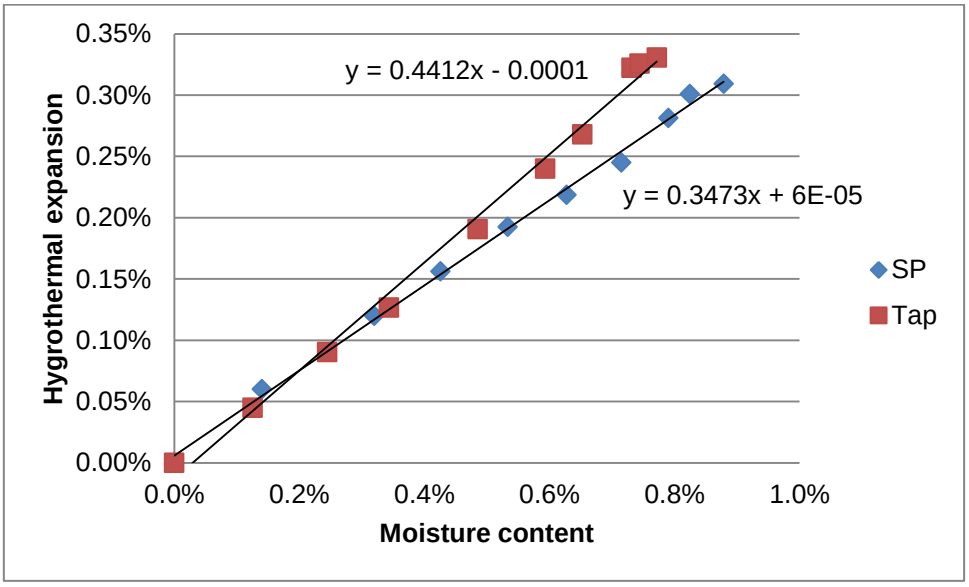

Fig.4. Hygrothermal expansion of UT $[90]_{16}$ laminate varying with moisture content.

2.3. Bending tests

The moisture content in composite laminates was saturated after 3-months of water immersion. In order to investigate the environmental effects on the mechanical properties in time domain, bending tests were carried out after 1-month and 3-months of water immersion. The experiments were conducted using 3-point bending according to the ISO standards [13, 14]. Typical loading force and displacement curves for the UD/UT/CP laminates in both dry and 3-M SP conditions are plot in Fig.5. The zigzag aspect can be seen in the curves of UD and CP laminates in dry condition; however the specimens showed a sudden break after immersion.

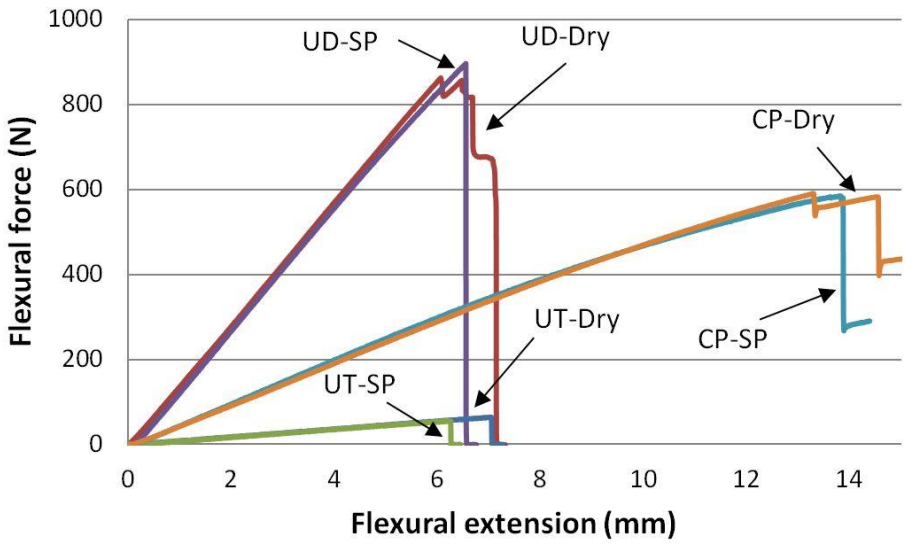

Fig.5. Typical flexural force-extension curves of UD/UT/CP laminates.

According to ISO 14130[13], the interlaminar shear strength can be determined by the maximum loading $F_{\max}$ and the specimen dimension (width 'w' and height 'h'),

$$\tau_{xz}^{app} = \frac{3}{4} \times \frac{F_{\max}}{wh} \qquad (1)$$

At least five samples in each group were tested, and the apparent interlaminar shear strength τ_{xz}^{app} (shown in Fig.6), apparent flexural strength σ_x^{app} and apparent flexural modulus E_f^{app} (shown in Table 3) were calculated. Please note that properties at 0-Month were measured prior to immersion so that they are independent of medium. So are the theoretical calculations.

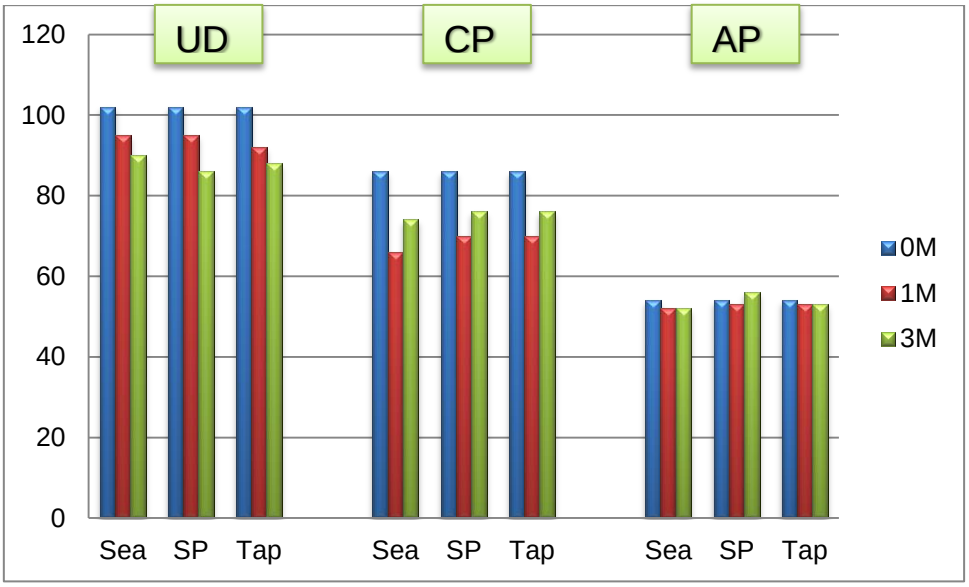

Fig.6. Measured ILSS (MPa) of UD/CP/AP laminates before (0M) and after moisture diffusion. 0-M: dry condition; 1-M: 1-month immersion; 3-M: 3-month immersion.

Table 3 Bending test results and their Standard Deviations (SDs)

	Immersion	$\sigma_x^{app}(MPa)$[b]		$E_f^{app}(GPa)$		
		0-M[a]	3-M	CLT[c]	0-M	3-M
UD	Sea	1598±56	1696±41	139	120±3	121±4
	SP		1780±122			121±4
	Tap		1688±137			122±2
UT	SP	117±5	99±6	8.8	8.4±0.3	9.1±0.1
	Tap		102±4			9.0±0.2
CP	Sea	1416±53	1441±40	62	56±2.2	58±0.4
	SP		1398±88			58±1.6
	Tap		1400±74			57±0.8

(a) 0-M: dry condition; 3-M: 3-month immersion.

(b) The values of UD and CP laminates were calculated with the 'large-deflection correction'.

(c) Calculated by Classical Laminate Theory (CLT) with the elastic properties shown in Table 4.

Because the deflections of the UD/UT laminates were close to the 'large-deflection criterion' (10%) and the deflection of CP laminate had exceeded the criterion, the flexural strength was then calculated by the 'large-deflection correction'[14],

$$\left(\sigma_{\max}^{f}\right)_{cor} = \frac{3F_{\max}L}{2wh^2}\left(1+6\left(\frac{D_{\max}}{L}\right)^2-3\left(\frac{D_{\max}h}{L^2}\right)\right) \quad (2)$$

The gradual degradation of interlaminar shear strength showed a similar trend with the work of Ryan et al [18]whose specimens contained the same epoxy system.

3. 3D FEA modelling of diffusion and bending

3.1. Moisture diffusion and hygrothermal expansion

It can be seen from Table 2 that the moisture diffusivity in the fibre direction is different from that in the transverse direction, so are the mechanical properties (elastic modulus, shear modulus and Poisson's ratio). Based on this orthotropic assumption, a 3D FEA model can be built using a rotated coordinate system to define the material properties of the off-axis plies,

$$\begin{pmatrix} x \\ y \end{pmatrix} = \begin{bmatrix} \cos(\theta) & -\sin(\theta) \\ \sin(\theta) & \cos(\theta) \end{bmatrix} \begin{pmatrix} X \\ Y \end{pmatrix} \quad (3)$$

where x and y are the original variables, X and Y are the transformed variables in the rotated (θ) coordinate system. The geometry and lay-up sequence of each group of laminates has been defined in Table 1.

In the experiments, the specimen was immersed into water, so all of the surfaces could be defined as being at the saturated moisture concentration. The saturated moisture concentration can be calculated by

$$c_{\max} = \frac{V\rho_c M_{\max}}{18\times10^{-3}V} = \frac{\rho_c M_{\max}}{18\times10^{-3}} \tag{4}$$

where ρ_c is the density of composite laminate, 18×10^{-3} is the molar mass of water with the unit kg/mol.

Substituting the saturated content $M_{\max} = 0.9\%$ from Table 2, and the density of CFRP composite $\rho_c = 1.6\times10^3 kg/m^3$, the saturated moisture concentration can be calculated as $c_{\max} = 800 mol/m^3$. This value is necessary for FEA boundary condition.

Once the moisture distribution is solved, the associated strain can be calculated from the coefficient of hygrothermal expansion (β). Because the moisture absorption has no effect on the fibre, the 'rule of mixture' should be used [3], and the principal CHE values at the lamina level can be calculated by

$$\begin{cases} \beta_1 = \dfrac{E_m}{E_1}\dfrac{\rho_c}{\rho_m}\beta_m \\ \beta_2 = (1+\nu_m)\dfrac{\rho_c}{\rho_m}\beta_m - \beta_1\nu_{12} \end{cases} \tag{5-1}$$

$$\rho_c = \rho_f V_{f+}\rho_m(1-V_f) \tag{5-2}$$

For many epoxy matrices, the β_m value is of the order of 0.32 [19], which is used in the present FEA model. Classical Laminate Theory (CLT) can be used to predict hygrothermal expansion in the off-axis laminates. Applying the 3D version of the transformation matrix into the CHE vector gives

$$\beta^k = T_\varepsilon \beta$$

$$T_\varepsilon = \begin{bmatrix} \cos^2\theta & \sin^2\theta & 0 & 0 & 0 & \cos\theta\sin\theta \\ \sin^2\theta & \cos^2\theta & 0 & 0 & 0 & -\cos\theta\sin\theta \\ 0 & 0 & 1 & 0 & 0 & 0 \\ 0 & 0 & 0 & \cos\theta & \sin\theta & 0 \\ 0 & 0 & 0 & -\sin\theta & \cos\theta & 0 \\ -2\cos\theta\sin\theta & 2\cos\theta\sin\theta & 0 & 0 & 0 & \cos^2\theta-\sin^2\theta \end{bmatrix} \tag{6}$$

Substituting equation (4) into the 3D version of CLT, the apparent CHE of laminate can be evaluated by equation (5) as described in [3],

$$\beta = aN^C = a\sum_{k=1}^{n}\overline{C}^k\beta^k t^k \tag{7}$$

where a is the 'a' block of the 'abbd' matrix; N^C is force per unit length caused by free moisture expansion; $\overline{C}^k$ is the full 3D stiffness matrix of the k^{th} ply; t^k is the thickness of the k^{th} ply. The 3D CLT formulae were solved by MATLAB [20].

The FEA solution gives the distribution of moisture concentration in 3D. Integration should be carried out to obtain the moisture content, and then hygrothermal expansion can be calculated by multiplying the coefficient of hygrothermal expansion with moisture content. Considering the inverse form of equation (2) in an infinite element, the expansion term can be expressed as

$$\varepsilon^{CHE} = \frac{18\times10^{-3}cV}{\rho_c V}\beta = \frac{18\times10^{-3}c\beta}{\rho_c} \qquad (8)$$

Equation (6) can be used to specify the coupling relation in the FEA model since the expansion term relates the moisture content (c) to mechanical expansion (ε^{CHE}). It should be noted that both the moisture content and the expansion are variable in time and space domains.

The elastic properties are then introduced to calculate the hygrothermal stresses. The mechanical properties and diffusion properties used in the FEA model are shown in Table 4.

Table 4 Material properties for moisture diffusion modelling

Longitudinal modulus E_1(GPa)	139
Transverse modulus $E_2 = E_3$(GPa)	8.8
In-plane shear modulus $G_{12} = G_{13}$(GPa)	4.7
Transverse shear modulus G_{23}(GPa)	3.0
In-plane Poisson's ratio $\nu_{12} = \nu_{13}$	0.26
Transverse Poisson's ratio ν_{23}	0.48
Longitudinal diffusivity $D_1(m^2/s)$	3.6×10^{-13}
Transverse diffusivity $D_2 = D_3(m^2/s)$	2.2×10^{-13}
Longitudinal CHE β_1	0
Transverse CHE $\beta_2 = \beta_3$	0.49

3.2. Hygrothermal stress coupled with bending

Due to the development of hygrothermal stresses after water absorption, the flexural stresses re-distribute when the composite laminates are subjected to bending. Therefore, the hygrothermal expansion was introduced as the initial strain in the mechanical model, and the diffusion/expansion were solved simultaneously. Since the diffusion (as well as the expansion) is time dependent, the mechanical model was solved in time domain, although the applied load was static.

The geometries used in the FEA models were the same as the test condition, and the maximum static loads evaluated in dry condition were applied in the mechanical model. The flexural strengths were investigated by long beam method [14], while the interlaminar shear stresses were investigated by short beam method [13]. Fig.7 shows the schematics of FEA model.

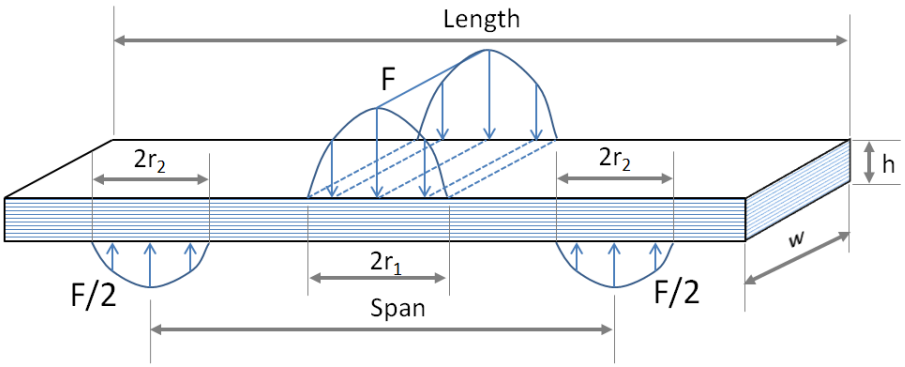

Fig.7. Illustration of the bending model

Reis' study[21] on the 3-point bending modelling reported the compressive broken of longitudinal fibre at the loading point when the contact was considered in the FEA model. The authors' previous paper [15] presented similar failure mechanism using sinusoidal distributions instead of contact condition shown in Fig.7, in order to minimise the stress concentration at the loading and support fixtures. The setup of the mechanical models and the mesh quality control have been presented previously [15].

Table 5 Geometries and boundary conditions in different groups of coupons

	UD		CP		AP
	Long beam	Short beam	Long beam	Short beam	Short beam
Length(mm)	100	20	100	20	20
Width(mm)	15	10	15	10	10
Height(mm)	2.08	2.08	1.92	1.92	1.92
Span(mm)	80	10	79	10	10
Force(N)	853	2933	574	2223	1395
r_1=r_2 (mm)	2				
c_{max} (mol/m^3)	800				

Table 5 shows the dimensions and loading forces for different groups of coupons. The height of specimen was adjusted to the 0.13mm for UD and 0.12 for CP/AP laminates in order to compensate the consistence of each ply. Once the FEA models were set up, the moisture distribution and the induced hygrothermal expansion inside laminate were investigated. The process of diffusion is very slow so that the moisture distribution varies in spatial and time domains. Additionally, the computing time (or DOFs) increased exponentially when the coupling term was introduced. Therefore, only 90 days of immersion were investigated. The FEA models were solved by COMSOL Multiphysics [22].

4. Results and discussions

4.1. Moisture diffusion and hygrothermal expansion

After 3-months accelerated water absorption, all of the specimens had become saturated. Table 2 has given the saturated moisture content of each group of specimens and their apparent moisture diffusivities. With the different geometries of UD and UT laminates, the longitudinal D_L and transverse D_T moisture diffusivities were calculated by Equation (A4), shown in the Appendix. It is shown that the moisture diffusion along fibre orientation (D_L) is about 60% faster than transverse direction (D_T).

Because the fibres do not absorb the moisture, the saturation is mainly dependent on the matrix and the fibre volume fraction. It has been known that the saturation and diffusivity are various for different polymer system. The typical saturation of polymer is epoxy 1.5%[12], vinyl ester 1.5%[23], polyester 1.5%[24], polyimide 4.4%[25] and PEEK 0.5%[26]. The diffusion test results of Ryan et al [18] gave a similar nominal saturation with the present work.

Fig.8 shows the water absorption in UD, UT, CP and AP laminates vs. square root (time). It can be seen that, within each lay-up, the saturated moisture content and the moisture diffusivity do not show noticeable differences between the sea water and tap water medium.

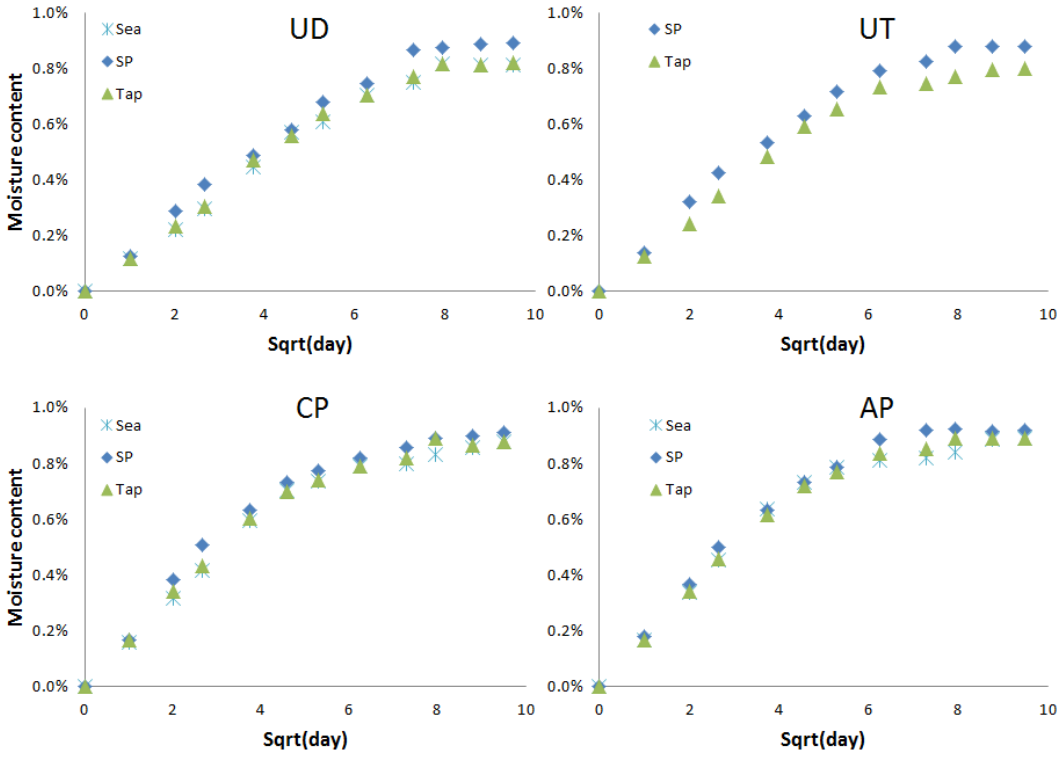

Fig.8. Moisture diffusion in UD/UT/CP/AP laminates immersed at 50°C sea water ('Sea'), tap water ('Tap') and sea water with 70bar hydrostatic pressure ('SP')

However the higher pressure induces a larger saturation in all four lay-ups. In the present case of 70 bar hydrostatic pressure, the saturation is 5% larger than that at ambient pressure. The

diffusion slope $(M_2 - M_1)/(\sqrt{t_2} - \sqrt{t_1})$ in the high pressure case is also larger. However, by substituting the diffusion slope and saturation into Equation (A2), it is found that the moisture diffusivity in the high pressure environment is the same as the normal pressure, as shown in Table 2.

The CP/AP laminates were cut from one composite plate, while the UD/UT laminates were cut from another plate. Therefore, the CP/AP laminates show similar results, as well as the UD/UT laminates. The calculated moisture diffusivities of the four lay-ups are shown in Table 2.

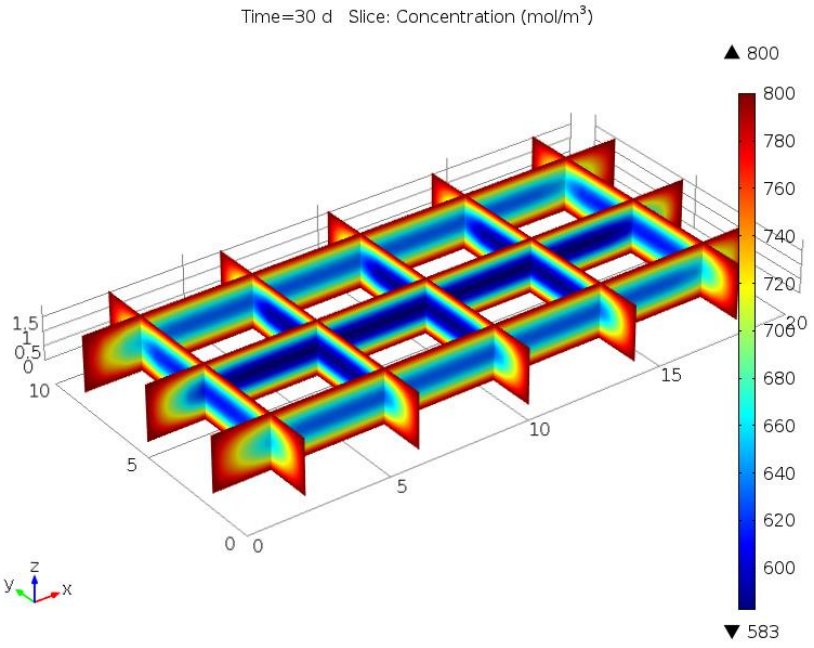

Fig.9. Moisture distribution according to FEA in AP short beam laminate after 30 days' water immersion (dimension unit: mm). The slice plot shows a smooth distribution of moisture concentration regardless of the ply orientations.

Although the longitudinal and transverse diffusivities show apparently different values, as shown in Table 2, the FEA modelling presented a smooth distribution of moisture concentration throughout the whole laminate with both complex lay-up (such as AP and CP laminates) and simple lay-up (such as UD and UT laminates). This is because the moisture diffusion is time dependent and the procedure is very slow. Fig.9 shows the FEA result for moisture distribution within an AP short beam laminate in slice-view after one month water immersion indicating different depth of water penetration in longitudinal and transverse. It can be seen that the moisture concentration distributed smoothly in the slice-section of xz-plane and yz-plane. Specifically, the moisture distribution through-thickness was extracted to analyse the effect of the longitudinal and transverse diffusivities, as shown in Fig.10. Fig.10 shows the moisture distribution on the mid-line of the AP laminate in the time domain, which indicates smooth distribution through-thickness regardless of the ply-orientation at different times. It can also be seen that the saturation occurs after 90 days of immersion.

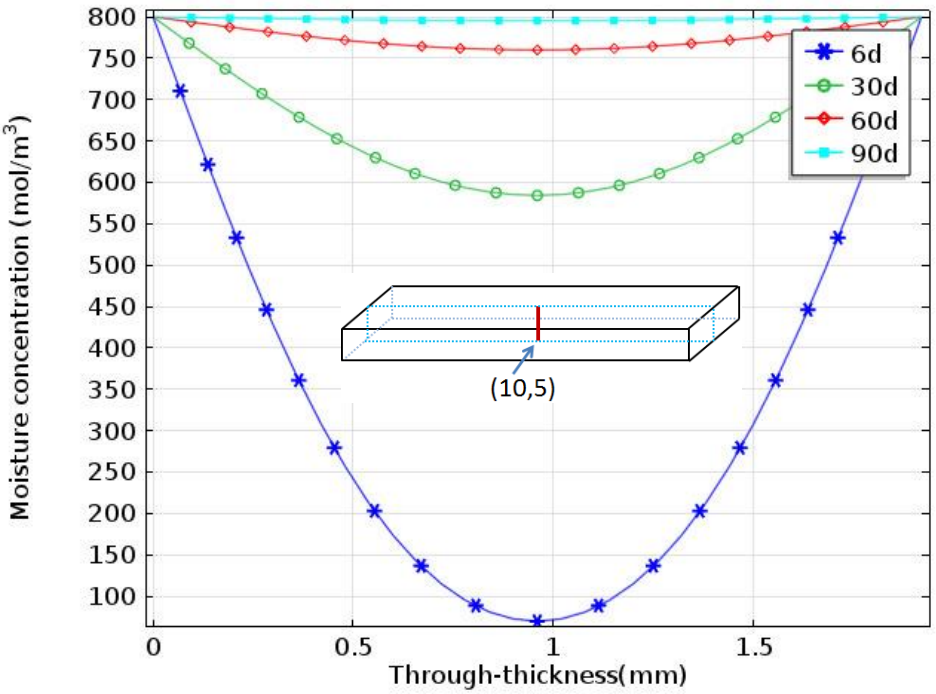

Fig.10. FEA moisture distribution of AP short beam laminate along the mid-line after 6/30/60/90 days' water immersion respectively. The moisture diffused smoothly inside the laminate, and converged to saturation.

The saturated hygrothermal expansion measured in the UT laminate showed a value of about 0.4% in tap water immersion (normalized to $M_{\max} = 0.9\%$), and a lower value (0.32%) in sea water with 70 bar hydrostatic pressure (SP), as shown in Fig. 1. One possible reason is that the hydrostatic pressure reduced the hygrothermal expansion. However, no measureable expansion was observed in UD/CP/AP laminates.

Substituting the saturated concentration, CHE and composite density in Equation (6), a reference transverse strain in an infinite unidirectional plate can be estimated to be

$$\varepsilon_T = \frac{18\times10^{-3} c_{\max} \beta_3}{\rho_c} = \frac{18\times10^{-3}\times800\times0.49}{1.6\times10^{3}} = 0.44\% .$$

In order to compare with this reference value, the hygrothermal strains of three types of laminates were extracted from the FEA simulations. Since the specimen was under free expansion induced by hygrothermal effects, the apparent normal strains can be extracted from the average normal displacements on the surfaces,

$$\begin{cases} \varepsilon_x = u_x \left(\frac{l}{2}\right)^{-1} \\ \varepsilon_y = u_y \left(\frac{w}{2}\right)^{-1} \\ \varepsilon_z = u_z \left(\frac{h}{2}\right)^{-1} \end{cases} \quad (9)$$

where ε_x, ε_y and ε_z are the apparent normal strains; u_x, u_y and u_z are the average normal displacements of yz, xz and xy surfaces;. $\frac{l}{2}, \frac{w}{2}$ and $\frac{h}{2}$ are the half-length, half-width and half-height of specimen respectively.

Fig.11 shows the expansion curves of UD/UT/CP/AP short beam laminates as a function of square root of time. It can be seen that the curves of UD/UT laminates are overlapped, so are the CP/AP laminates. It is noted that the maximum hygrothermal expansion of UD/UT laminates is in line with the reference value (0.44%) but CP/AP laminates have significantly higher values.

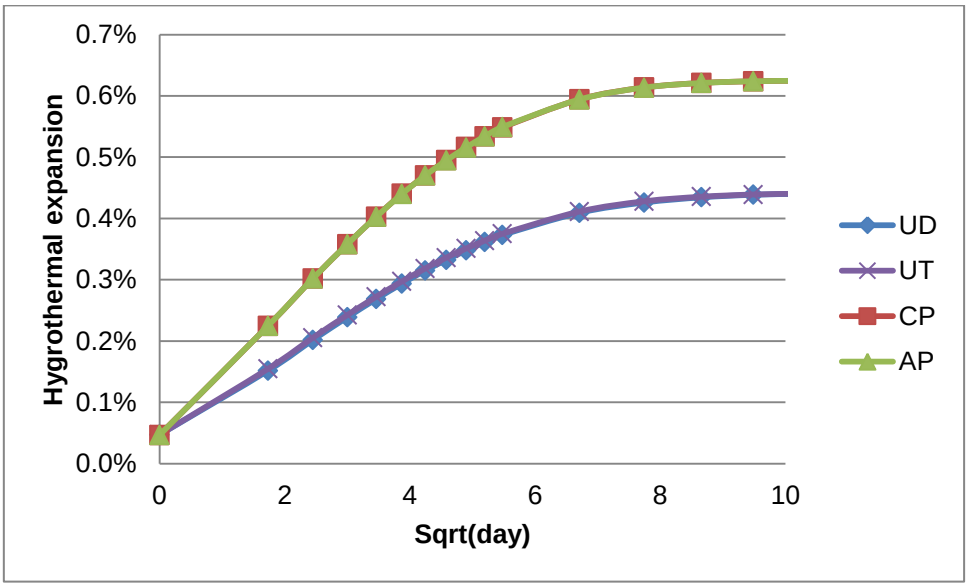

Fig.11. FEA out-of-plane hygrothermal expansion of UD/UT/CP/AP short beam laminates

The CLT calculation of laminate CHE can explain this increase of expansion in CP/AP laminates. Applying Equations (4-5) to CP laminate, the apparent CHE can be calculated giving $\beta_x = \beta_y = 0.04, \beta_z = 0.70$. The predicted out-of-plane CHE value (β_z) is in line with the maximum CHE extracted from FEA simulations shown in Fig.11.

4.2 Hygrothermal stresses and edge effect

In the FEA model, the concentration on all surfaces was constant during the entire diffusion process. The hygrothermal stresses were induced in 'free edge' region at the very beginning, and then the stresses propagated inside the specimen following the moisture diffusion. Fig.12 shows the through-thickness distribution of interlaminar shear stress (τ_{13}) within the AP short beam laminate after one month's diffusion. It can be seen that the interlaminar shear stress induced by hygrothermal expansion could be as high as the 20% of the interlaminar shear strength (as shown in Fig.6). This high value of stress might induce the stress re-distribution when the laminate is subjected to mechanical loading. However, this induced interlaminar shear stress only appeared at the interfaces of plies and decayed rapidly inside the laminate and finally converged to zero in the centre. The coupling of the hygrothermal stress with bending will be discussed in the next section.

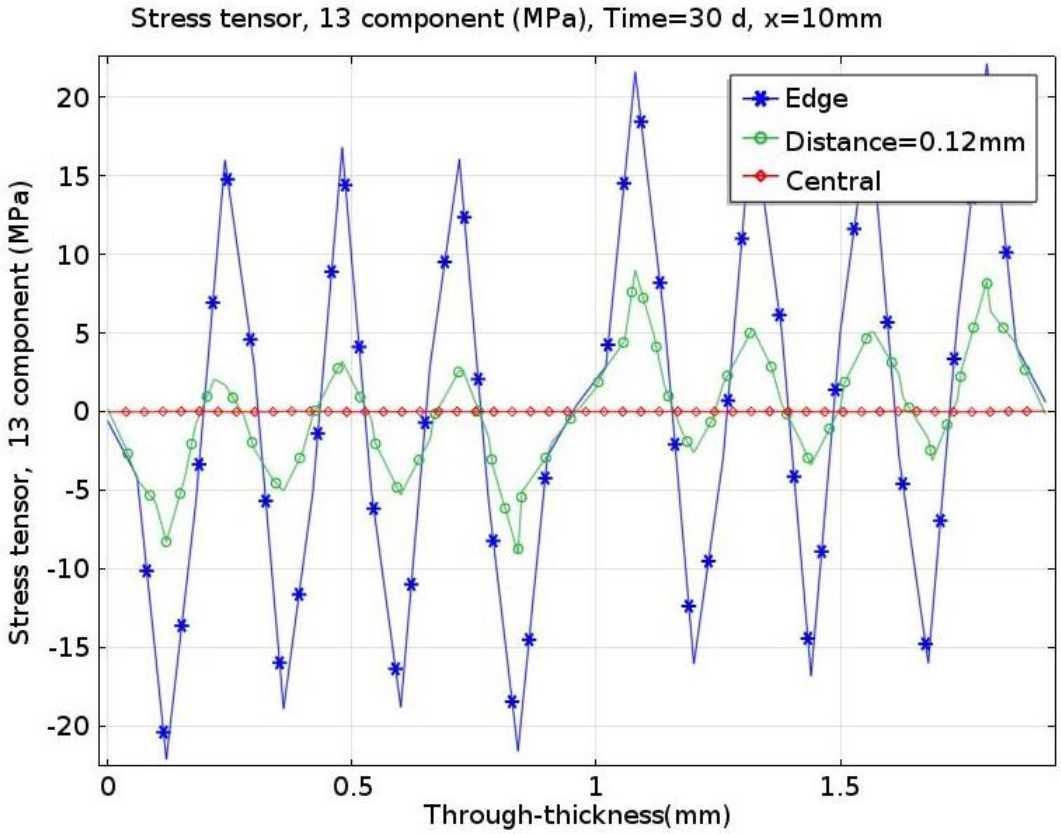

Fig.12. FEA result for interlaminar shear stress τ_{13} induced by hygrothermal effect in AP short beam laminate after one month's diffusion

Such a strong 'free edge' effect can also be found in the CP laminate. Fig.13 shows the surface plot of interlaminar shear stress τ_{13} in the CP short beam laminate. Compared with the interlaminar shear strength measured in dry condition, this induced stress τ_{13} was so high that it could not be neglected in the context of fracture or fatigue initiation. Additionally, this induced shear stress τ_{13} would reduce the measured interlaminar shear strength significantly, as shown in Fig.6.

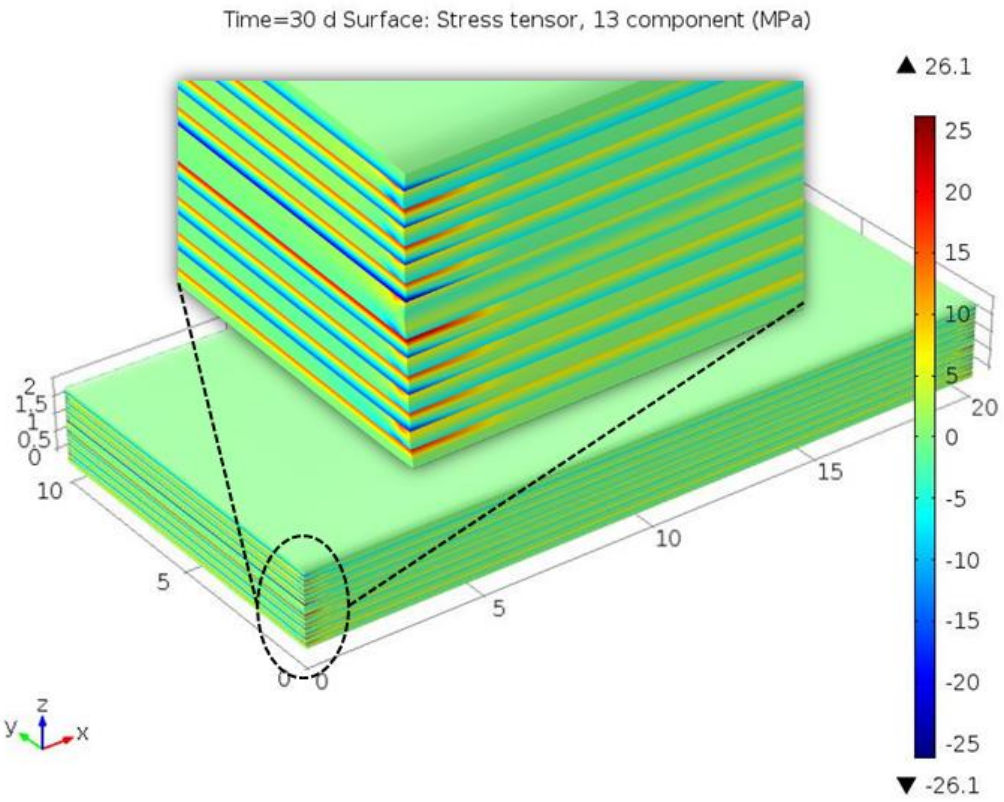

Fig.13. FEA result for interlaminar shear stress τ_{13} induced by hygrothermal expansion in CP short beam laminate after one month's water absorption.

In the previous section, the 'free edge' effect induced by hygrothermal expansion was observed in 3D FEA model. It showed the induced interlaminar shear stress τ_{13} is of the order of 20 MPa in CP/AP laminate. Transverse normal stresses are also as high as: 30 MPa (σ_2 or σ_3) in CP/AP laminates and 10 MPa (σ_2 or σ_3) in UD/UT laminates. And this edge effect decayed rapidly inside the laminate within a couple of ply-thickness.

The FEA model introduced this hygrothermal expansion as the initial strain. When the bending condition was applied, this effect would be coupled with the bending stress leading to stress re-distribution. Due to the small deformation in FEA model, the diffusion and expansion could be considered as a one-way coupling problem: the effect of structural deformation on moisture diffusion was not considered in FEA model. Therefore, the time dependent diffusion was the same as the case without bending. On the other hand, the hygrothermal stresses shown in the case of 'free expansion' were coupled with the bending stresses. Fig.14 shows the time dependent distribution of transverse normal stress in CP short beam laminate. With the increase of moisture content in laminate, the hygrothermal stress showed an increasing trend with the concentration.

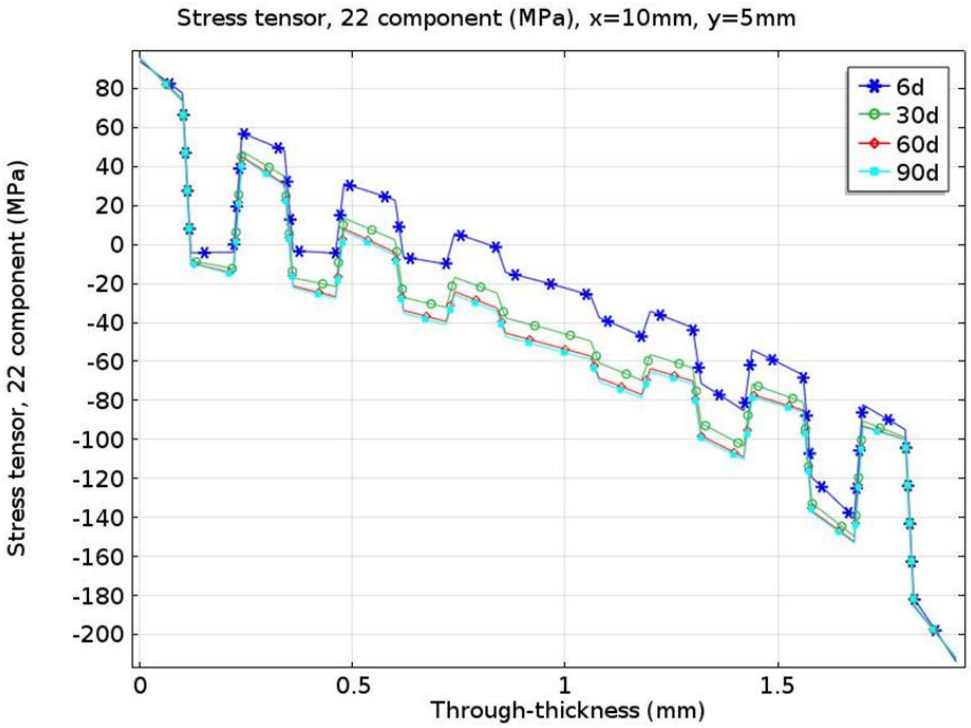

Fig.14. FEA through-thickness distribution of σ_2 at central point (x=10mm, y=5mm) of CP short beam laminate in the time domain. The transverse stress shifts into compression.

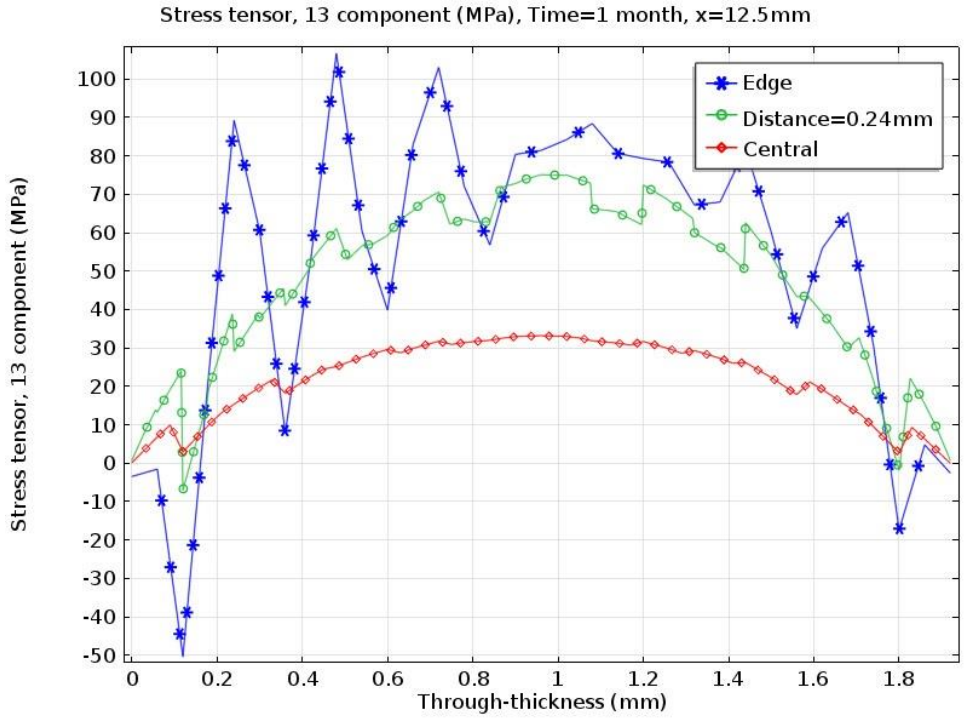

Fig.15. FEA through-thickness distribution of τ_{13} after one month's diffusion in AP short beam laminate

Fig.15 shows the through-thickness distribution of interlaminar shear stress (τ_{13}) of the AP short beam laminate. Compared with the dry condition (shown in [15]), the coupling had no

effect on the maximum value of τ_{13}. However, the stress was asymmetric about the mid-plane, and the positions of peaks shifted to the bottom side.

Fig.16 gives a typical failure image of AP laminate from a bending test. The sample was immersed for one month in tap water. Compared with the dry condition, more cracks were found on the bottom side and the cracks propagated a longer distance inside the laminate. However, the interlaminar shear strength of the AP laminate showed a small variation due to the water immersion.

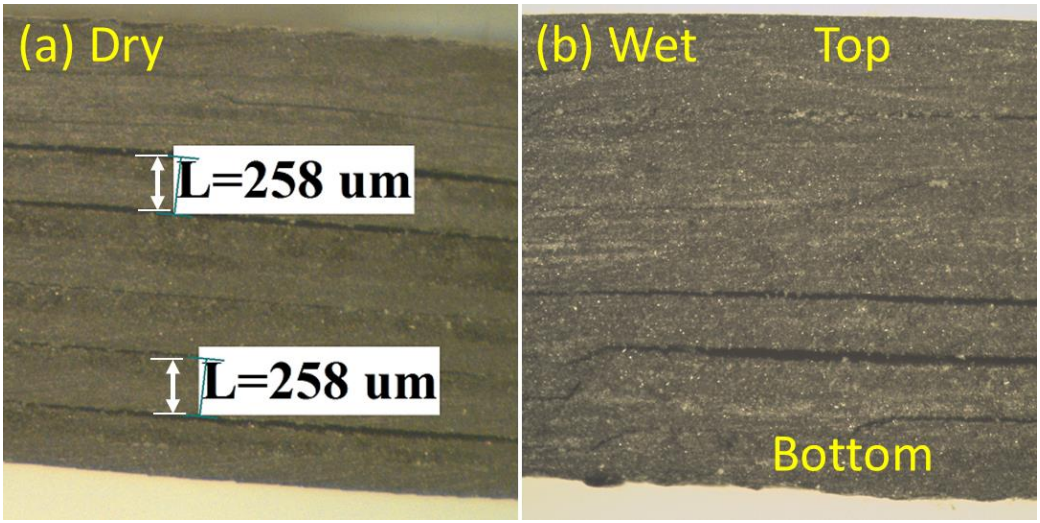

Fig.16. Typical failure image of AP short beam laminate in ILSS test (side view). (a) in dry condition; (b) after one month's tap water immersion.

Fig.6 has shown the measured ILSS after three kinds of water immersion. The samples were taken out of the chambers for bending test after 1 month or 3 months' immersion. The AP laminate showed a consistent value of ILSS for all the immersion conditions, and no degradation of this property was found. However, it showed quite a different failure mode from the dry condition, due to the hygrothermal expansion. Withstanding the same level of bending load, the AP laminate presented much larger cracks after water immersion, and more cracks appeared on the bottom side, as shown in Fig.16. This is because the peak values of interlaminar shear stress shift to the bottom side, which has been shown in the FEA results in Fig.15.

The ILSS of the CP laminate showed a sharp reduction (20%) after 1 month immersion and a slight increase after 3 months immersion. However, regardless of the three kinds of medium, the ILSS of CP laminate remained at the same level with respect to immersion time (0/1/3 month), which is similar to the UD and AP laminates.

The ILSS of the UD laminate showed a gradual decrease from 1 month to 3 months water absorption, but no significant difference among the three kinds of medium was observed. It was found that, compared with the interlaminar failure in dry condition, the UD laminate failed by the plastic deformation after water absorption. Fig.17 shows a typical failure image of UD short beam laminate. The laminate shown in Figure 17b was immersed in sea water for

1 month before being tested in bending. A large number of micro cracks were found in the optical microscope image.

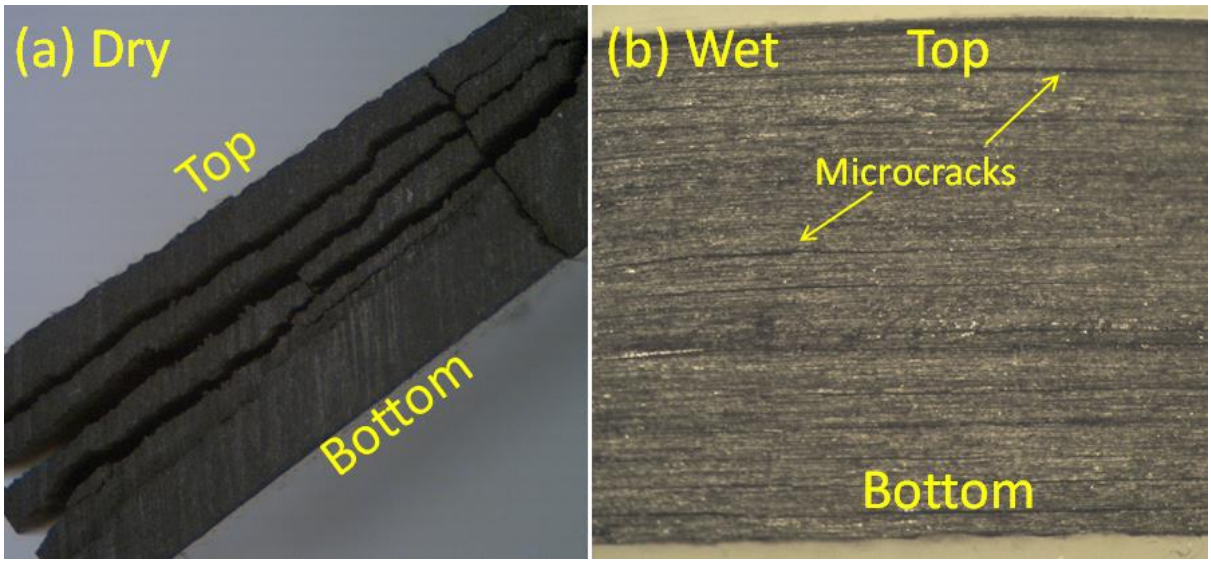

Fig.17. Typical failure image of UD short beam laminate in ILSS bending test (side view): (a) in dry condition, (b) after 1-month's water immersion. The delamination was uncompleted in wet condition (b).

4.3 Flexural stress and modulus

According to the previous 3D FEA study [15], the UD laminate failed by compression in bending condition, and the flexural strength was the same as the laminate compressive strength in uniaxial compression. If the thermal residual stress is taken into account, the composite laminate was subjected to initial compression in the dry condition. When the composite laminates were immersed, the hygrothermal expansion should relax the thermal residual stress. As a consequence, the UD laminate showed a relative higher flexural strength in bending after moisture absorption. Fig.18 shows the normalized flexural strength of CP/UD/UT laminates in three kinds of water immersions. The flexural strength of UD laminate showed a 5%-10% increase (of the order of 100 MPa) compared to that in dry condition.

Although many researchers have investigated the degradation of the moisture ingress, most of them have focused on either tension or compression. Some researchers had reported that the tensile strength showed gradual decrease with increasing immersion time [4, 18, 27]. In bending, composite laminates are subjected to tension, compression and shear, which is quite different from the uniaxial tension and compression. Therefore, bending test represents more general condition, and the change of stress distribution contributed significantly to the failure mechanisms.

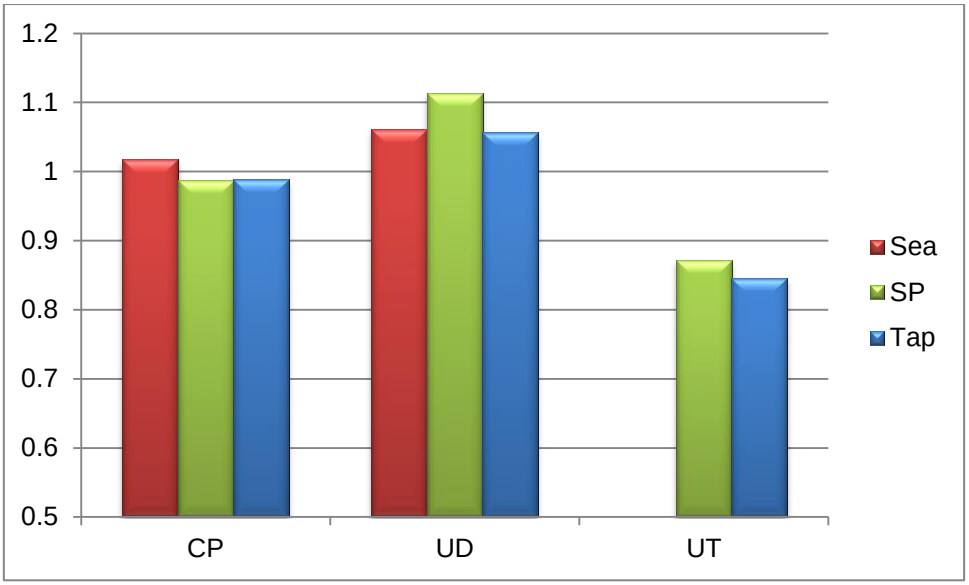

Fig.18. Flexural strength of CP/UD/UT laminates after 3-month's water absorption. The values were normalized by the measurement in dry condition.

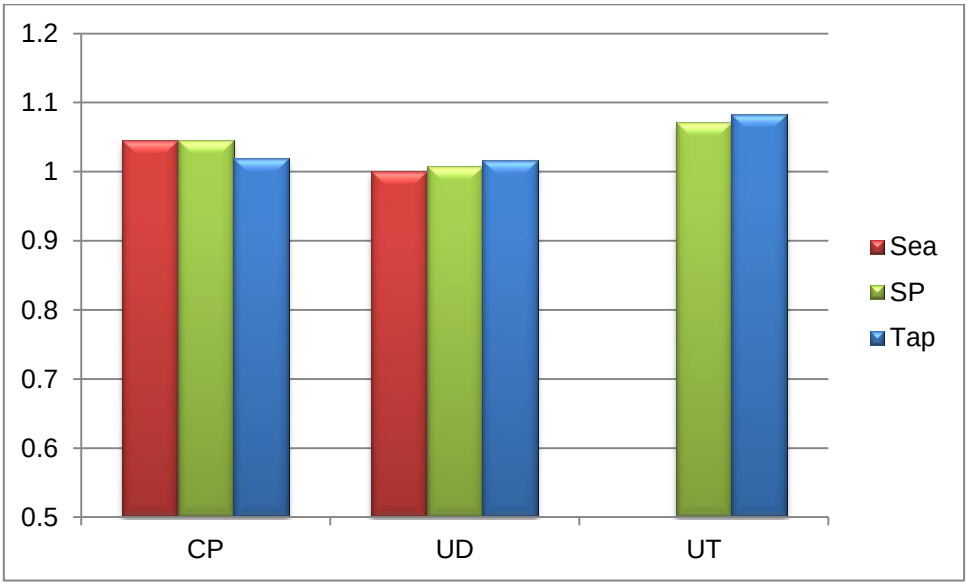

Fig.19. Flexural modulus of CP/UD/UT laminates after 3-month's water absorption. The values were normalized by the measurement in dry condition.

On the other hand, the flexural strength of UT laminate showed a dramatic decrease after moisture diffusion, while the CP laminate retained the flexural strength of the dry condition. Since the failure mechanism of UT laminate was matrix dominated, the flexural strength was strongly dependent on the bonded interface between matrix and fibre.

Fig.19 shows the normalized flexural moduli of CP/UD/UT laminates in three kinds of water immersions. It can be seen that the flexural modulus of CP/UD laminates had a small fluctuation after moisture absorption, however, the UT laminate showed an opposite trend to its strength. Compared to the decrease in flexural strength shown in Fig.16, the UT laminate became stiffer after moisture absorption. One possible reason is because the epoxy became

stiffer when the water molecules diffuse inside the long molecular chain of polymer. The chemical structure of epoxy resin was shown in Fig.1. Due to the competition of sulfone bridge, the electron density of nitrogen-carbon bond between DDS and DGEBA is relatively low which leads to water resistance of DDS unit[28]. According to reference[29], the propagation rate constant for hydrocarbon oxidation in propanol unit is higher than the one in isopropyledene unit, which means that the hydroxyl radical in DGEBA exhibits relatively more hydrophilic. As a consequence, the water molecular was mainly absorbed by the sub-branch (OH-) of DGEBA which had no effect on strength of the cross-link network but might slightly enhance the stiffness of the resin. Therefore, the decrease of strength observed in UT laminate might be caused by the degradation of fibre/matrix interface which will be discussed in section 4.5.

Scanning eletronic microscopy (SEM) was used to examine the interface of fibre/epoxy at the fracture surface. The fracture debris was taken from UT laminate, and dry/tap/sea conditions were examined. The samples were coated with gold/paladium before being examined in SEM. Fig.20-22 show the particular fracture surfaces of the three conditions. There are two magnifications in each figure, 500 times and 4000 times.

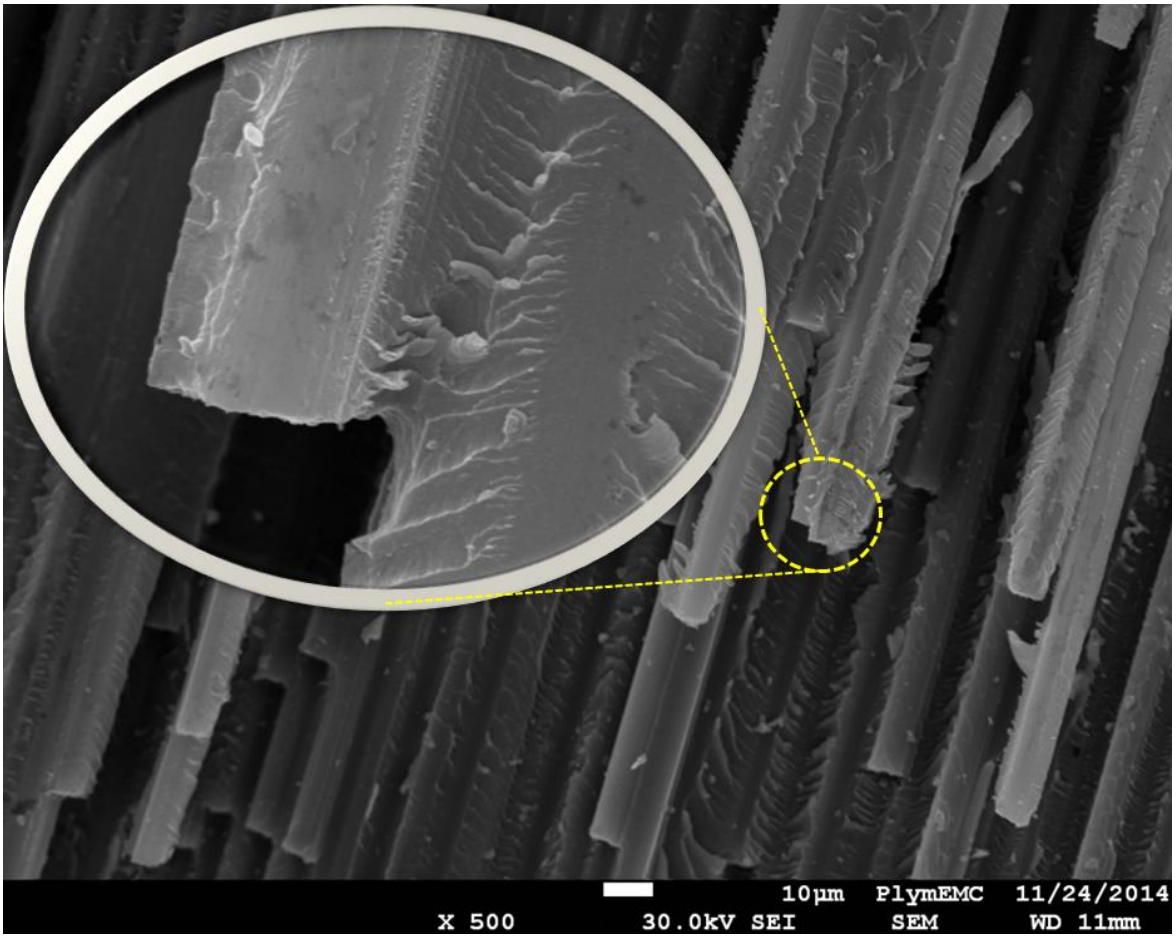

Fig.20. SEM image of dry sample with a local magnification

Fig.20 illustrates the transverse fracture surface within a dry condition UT sample. The epoxy was still attached to the carbon fibre, so that the fractured polymer showed a tough wave-like

morphology. Without water ingression, the epoxy provided adequate adhesion to the carbon fibre, and the failure mode tended to be the tensile fracture of epoxy rather than the debonding of fibre/epoxy interphase.

Fig.21 and Fig.22 show similar characters of transverse fracture surface of tap water and sea water conditions. At a lower magnification, it can be seen in Fig.21 that the epoxy became porous; however the wave-like morphology was still observed which indicates that the failure mode was the tensile fracture of epoxy. At a higher magnification in Fig.22, the carbon fibre showed sections of bare surface which indicates that the adhesion of epoxy on carbon fibre had deteriorated after water absorption.

It should be noted that the SEM could only examine a local area under a relative high magnification. It was found that, in sea water condition, the number of bare fibres was higher than the tap water condition. Therefore, it is reasonable to believe that the degradation in sea water is more severe in long term exposure.

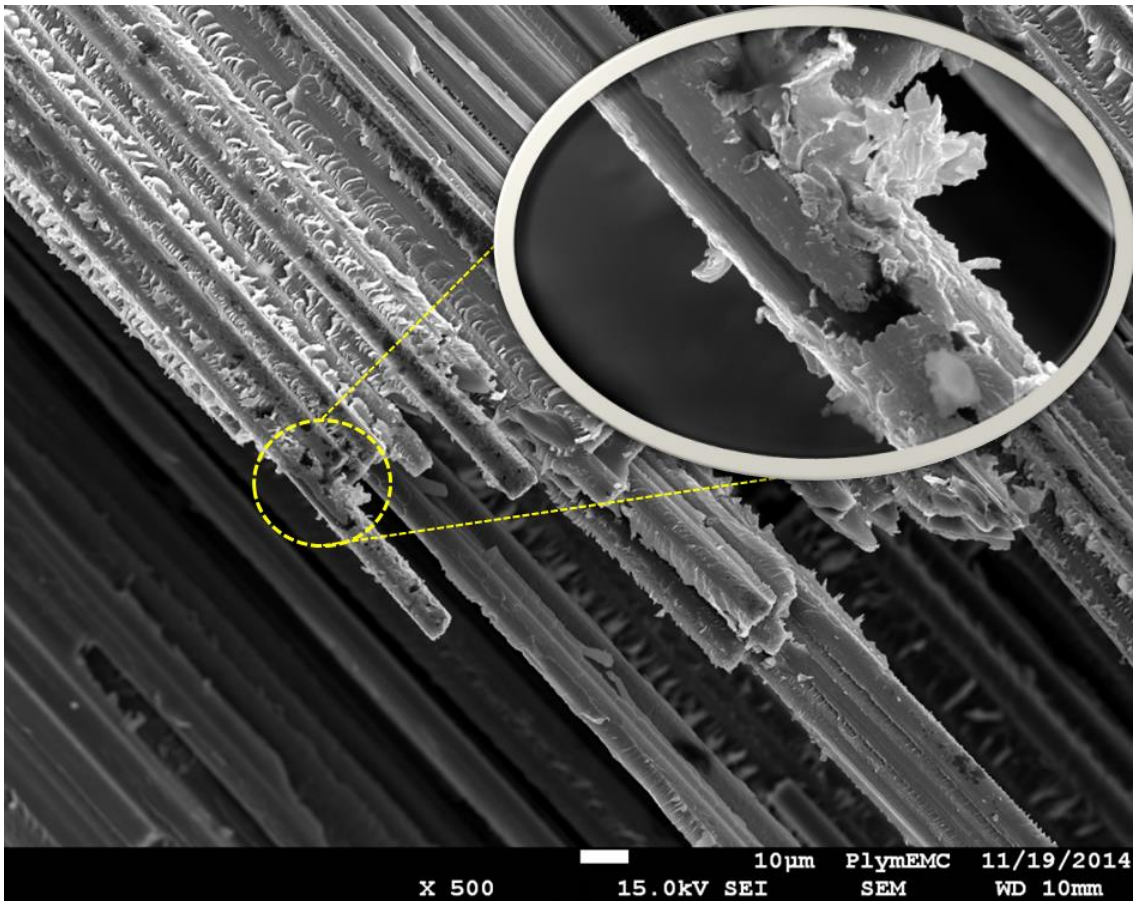

Fig.21. SEM image of tap water condition

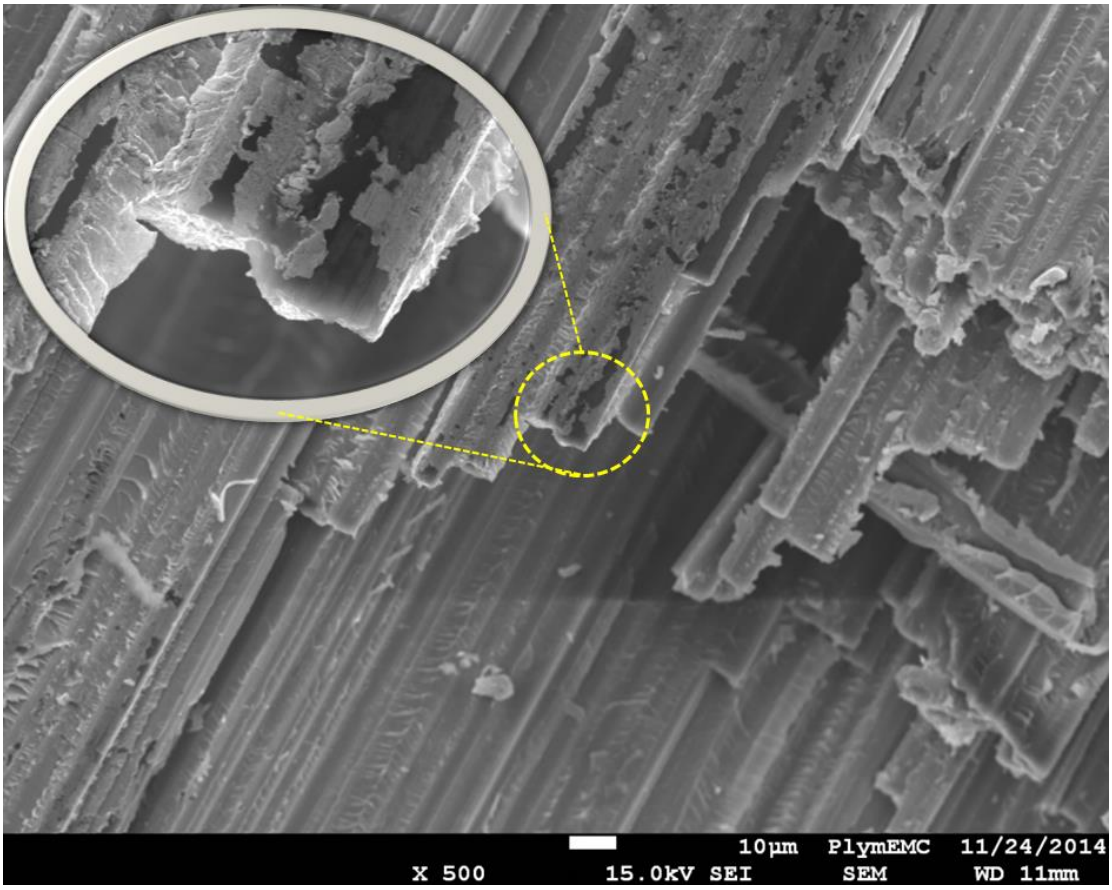

Fig.22. SEM image of sea water condition

5 Conclusions

Composite structures exposed in marine environment are subjected to many aspects, among which this paper has investigated the effects of water immersions on the CFRP composites. A robust 3D FEA model has been developed to analyse the hygrothermal effects. The experimental results showed a good agreement with the FEA solutions, which has also been validated by CLT calculation. Some findings are concluded according to the study:

a) The moisture diffusivity in the Tap/Sea/SP water immersions showed negligible difference at the same temperature. Although the longitudinal moisture diffusivity presented a much higher value than the transverse diffusivity (60% in this study), the moisture diffusion in composite laminates showed a smooth distribution through thickness regardless of ply orientation.
b) Hygrothermal stresses could be induced at the very beginning of diffusion, and these stresses mainly appeared at the edge region (edge effect) which means that the laminate lay-up becomes a critical issue for the exposed surfaces. For interlaminar shear stress, the induced hygrothermal stress could be as high as 20% of the strength. Therefore, in the design of marine composites, it is desirable to avoid complicated lay-ups at the connection region of composite joints or notches in order to improve the fatigue properties.

c) The water absorption had no significant effects on the strength of DGEBA-DDS cross-link system (i.e. 977-2 epoxy resin). However, the composite strength was reduced significantly due to the degradation of fibre/matrix interface, and it was observed that the degradation of interface in sea water was more significant than in fresh water.
d) The SEM analysis has shown a variety of matrix fracture morphologies and the degradation of fibre/matrix interface increases the risk of interface debonding in CFRP composites in simulated marine environment.

6 Acknowledgement

The authors would like to thank Professor Long-yuan Li for his advice on FEA modelling, Dr Richard Cullen for his kind help with composites manufacturing, Terry Richards for his support of the mechanical tests, and the financial support of the School of Marine Science and Engineering, Plymouth University.

7 Reference

1. Greene, E., *Marine composites*. 1999: Eric Greene Associates.
2. Hull, D. and T. Clyne, *An introduction to composite materials*. 1996: Cambridge university press.
3. Gibson, R.F., *Principles of composite materials mechanics.* McGraw-Hill, 1994(ISBN O-07-023451-5).
4. Zafar, A., et al., *Investigation of the long term effects of moisture on carbon fibre and epoxy matrix composites.* Composites Science and Technology, 2012. **72**(6): p. 656-666.
5. Smith, W.F. and J. Hashemi, *Foundations of materials science and engineering*. 2006: Mcgraw-Hill Publishing.
6. Shen, C.-H. and G.S. Springer, *Moisture absorption and desorption of composite materials.* Journal of Composite Materials, 1976. **10**(1): p. 2-20.
7. Vinson, J.R., *Advanced composite materials-environmental effects*. 1978: ASTM International.
8. Cairns, D.S. and D.F. Adams, *Moisture and thermal expansion of composite materials.* U,S. ARMY RESEARCH OFFICE Report, 1981. **UWME-DR-101-104-1**.
9. Springer, G.S., *Environmental effects on composite materials*. Vol. 2. 1981: Technomic Pennsylvania.
10. Cairns, D. and D. Adams, *Moisture and thermal expansion properties of unidirectional composite materials and the epoxy matrix.* Environmental Effects on Composite Materials, 1984. **2**: p. 300-316.
11. Rasoldier, N., et al., *Model systems for thermo-oxidised epoxy composite matrices.* Composites Part A: Applied Science and Manufacturing, 2008. **39**(9): p. 1522-1529.
12. Cytec, *CYCOM 977-2 Epoxy resin system. www.cytec.com.* Technical data sheet, 2012.
13. ISO, B., *14130.* Fibre-Reinforced Plastic Composites—Determina tion of Apparent Interlaminar Shear Strength by Short-Beam, 1998.
14. ISO, I., *14125: 1998 (E).* Fibre reinforced plastic composites–determination of flexural properties, 1998.
15. Meng, M., et al., *3D FEA modelling of laminated composites in bending and their failure mechanisms.* Composite Structures, 2015. **119**(0): p. 693-708.
16. D1141-98, A., *Standard Practice for the Preparation of Substitute Ocean Water*. 2008, ASTM International West Conshohocken, PA.

17. D5229/D5229M, A., *Standard Test Method for Moisture Absorption Properties and Equilibrium Conditioning of Polymer Matrix Composite Materials*, in *ASTM*. 2004. p. 13.
18. Ryan, J., R. Adams, and S. Brown. *Moisture ingress effect on properties of CFRP*. in *Proceedings of the 17th International Conference on Composite Materials (ICCM'09)*. 2009.
19. Walrath, D.E. and D.F. Adams, *Fatigue Behavior of Hercules 3501-6 Epoxy Resin*. 1980, DTIC Document.
20. MATWORKS, *MATLAB reference manual.* 2013.
21. Reis, P.N.B., et al., *Flexural behaviour of hybrid laminated composites.* Composites Part A: Applied Science and Manufacturing, 2007. **38**(6): p. 1612-1620.
22. COMSOL, *COMSOL Multiphysics reference manual.* 2013.
23. Derakane, *Derakane 411-45 Epoxy Vinyl Ester resin. www.ashland.com.* Technical data sheet, 2011.
24. Davallo, M., H. Pasdar, and M. Mohseni, *Mechanical Properties of Unsaturated Polyester Resin.* International Journal of ChemTech Research, 2010. **2**(4): p. 2113-2117.
25. Cytec, *CYCOM 2237 Polyimide resin system. www.cytec.com.* Technical data sheet, 2012.
26. Victrex, *Victrex PEEK polymer. www.victrex.com.* Technical data sheet, 2012.
27. Kootsookos, A. and A.P. Mouritz, *Seawater durability of glass- and carbon-polymer composites.* Composites Science and Technology, 2004. **64**(10–11): p. 1503-1511.
28. EICHLER, J. and J. MLEZIVA, *STUDY ON REACTIVITY OF AROMATIC DIAMINES WITH EPOXIDE RESINS.* ANGEWANDTE MAKROMOLEKULARE CHEMIE, 1971. **19**(NSEP): p. 31-&.
29. Korcek, S., et al., *Absolute rate constants for hydrocarbon autoxidation. XXI. Activation energies for propagation and the correlation of propagation rate constants with carbon-hydrogen bond strengths.* Canadian Journal of Chemistry, 1972. **50**(14): p. 2285-2297.
30. Gigliotti, M., et al. *Modelling and experimental characterisation of hygrothermoelastic stress in polymer matrix composites*. in *Macromolecular Symposia*. 2007. Wiley Online Library.
31. Pomies, F., L. Carlsson, and J. Gillespie, *Marine environmental effects on polymer matrix composites.* ASTM SPECIAL TECHNICAL PUBLICATION, 1995. **1230**: p. 283-303.

Appendix

According to the previous study [3], the moisture diffusivity of composites can be expressed as an exponent function of the environmental temperature (known as an Arrhenius relation),

$$D = D_0 \exp\left(\frac{-E_a}{RT}\right) \tag{A1}$$

where $R = 8.31 J \cdot mol^{-1} \cdot K^{-1}$ is the gas constant; D_0 is a material constant; and E_a is the activation energy for diffusion.

Since the carbon fibre is assumed not to absorb moisture, the composite's moisture diffusivity is mainly dependent on the polymer. A previous study [30] provides the reference parameters of Equation (A1) for 977-2 epoxy: $D_0 = 2\times10^{-9} m^2 s^{-1}$, $E_a / R = 2910 K^{-1}$. Therefore, the moisture diffusivity of HTS/977-2 can be roughly estimated of the order of $3\times10^{-13} m^2/s$ in the present case (50°C). According to ASTM D5229 [17], the reference time period for each measurement is established by $0.02h^2/D$, giving an approximate interval of 5 days.

Fick's laws were applied to calculate the apparent moisture diffusivity (D^{app}) once the saturated moisture content ($M_{\max}$) is estimated [17],

$$D^{app} = \pi\left(\frac{h}{4M_{\max}}\right)^2\left(\frac{M_2 - M_1}{\sqrt{t_2} - \sqrt{t_1}}\right)^2 \tag{A2.1}$$

$$M = M_{\max}\left[1 - \exp\left(-7.3\left(\frac{D^{app}t}{h^2}\right)^{0.75}\right)\right] \tag{A2.2}$$

where h is the specimen thickness; M is the specimen moisture content (%); t is the absorption time; $(M_2 - M_1)/\left(\sqrt{t_2} - \sqrt{t_1}\right)$ is the slope of moisture absorption plot in the initial linear portion of the curve.

Like the orthotropic elastic properties in laminated composites, the previous study had reported that diffusion properties also show orthotropic[31]. Fig.22 is an illustration of the longitudinal and transverse moisture diffusivities in both micro and macro scales.

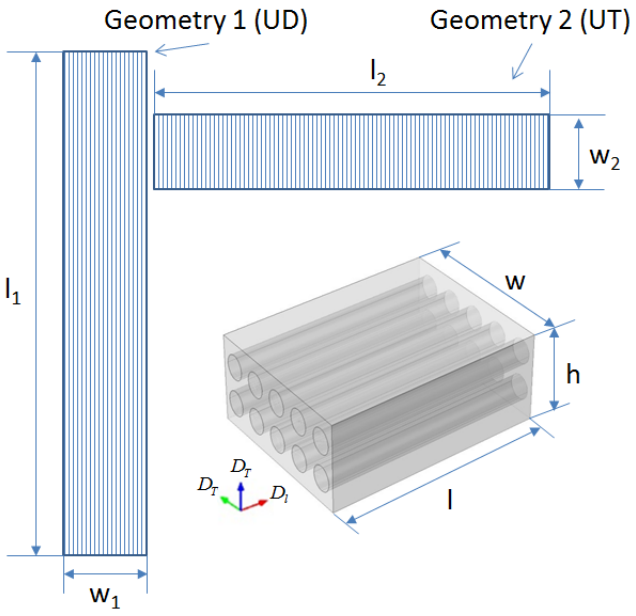

Fig.23. Orthotropic moisture diffusivity assumption and the two geometries for the calculation of longitudinal and transverse diffusivities.

If the specimen dimension is finite (which is happening in present case), the longitudinal and transverse moisture diffusivities should be used to compensate the edge correction [31],

$$\sqrt{D^{app}} = \frac{w+h}{w}\sqrt{D_T} + \frac{h}{l}\sqrt{D_L} \tag{A3}$$

The apparent diffusivity D^{app} is determined by Equation (A2), while D_L and D_T can be determined by two different geometric samples,

$$\begin{cases} D_T = \left(l_1\sqrt{D_1^{app}} - l_2\sqrt{D_2^{app}}\right)^2 \cdot \left(\frac{w_1+h}{w_1}\cdot l_1 - \frac{w_2+h}{w_2}\cdot l_2\right)^{-2} \\ D_L = \left[\frac{l_1}{h}\left(\sqrt{D_1^{app}} - \frac{w_1+h}{w_1}\sqrt{D_T}\right)\right]^2 \end{cases} \tag{A4.1}$$

With a very long length l and short width w (as in the UD laminate), Equation (A3) is reduced to

$$\sqrt{D_1^{app}} = \frac{w_1+h}{w_1}\sqrt{D_T} \tag{A4.2}$$

With a very long width w and short length l (as in the UT laminate), Equation (A3) is reduced to

$$\sqrt{D_2^{app}} = \sqrt{D_T} + \frac{h}{l_2}\sqrt{D_L} \tag{A4.3}$$